applied sciences

MDPI

Article

Experimental Validation of the Statistical Properties of Speckled-Speckle Fields in the Mesoscopic Intensity Regime

Camilla Bianciardi [1,†], Alessia Allevi [2,*,†] and Maria Bondani [3,†]

[1] Department of Science and High Technology, University of Insubria, Via Valleggio 11, I-22100 Como, Italy
[2] Department of Science and High Technology, University of Insubria and Institute for Photonics and Nanotechnologies, IFN-CNR, Via Valleggio 11, I-22100 Como, Italy
[3] Institute for Photonics and Nanotechnologies, IFN-CNR, Via Valleggio 11, I-22100 Como, Italy
* Correspondence: alessia.allevi@uninsubria.it; Tel.: +39-031-238-6253
† These authors contributed equally to this work.

Abstract: Several imaging techniques, such as ghost imaging, are based on the use of classical and quantum correlated light states. This fact has encouraged the search for new strategies to produce light states more correlated than the thermal states that are typically used. In this work, we produce and characterize classical states of light with "more than thermal" statistics. Such states are obtained by means of a sequence of two rotating ground-glass disks and by appropriately selecting the speckle field produced at the output of each disk. The experimental results are in excellent agreement with the developed theoretical model, suggesting the potential of this kind of light for imaging applications.

Keywords: superthermal light; photon-number statistics; mesoscopic intensity regime; photon-number-resolving detectors

Citation: Bianciardi, C.; Allevi, A.; Bondani, M. Experimental Validation of the Statistical Properties of Speckled-Speckle Fields in the Mesoscopic Intensity Regime. *Appl. Sci.* **2023**, *13*, 4490. https://doi.org/10.3390/app13074490

Academic Editor: Leonid Burakovsky

Received: 16 February 2023
Revised: 21 March 2023
Accepted: 30 March 2023
Published: 1 April 2023

1. Introduction

The existence of intensity fluctuations in light sources is a useful resource for imaging applications. Indeed, there are imaging techniques, such as ghost imaging, whose working principle relies on the spatial correlations coming from the intensity fluctuations [1,2]. The most common classical light source exhibiting such a feature is the pseudo-thermal light, typically obtained by passing a laser beam through a rotating ground-glass disk [3], which shows the so-called speckle field, consisting of many spatial modes [4]. Many realizations of this type of light in different intensity domains [5–9] have been exploited to address imaging protocols, reconstructing correlation images of different kinds of objects, including faint and photolabile ones [10,11]. Indeed, the use of non-invasive methods for observing various physical and biological activities employing structured patterns, such as speckle patterns, represents a hot topic in the imaging context [12,13]. The quality of the reconstructed images is usually quantified in terms of some figures of merit, such as the contrast and the signal-to-noise ratio [10,14–16]. The values of these estimators can be increased by the use of light sources characterized by intensity fluctuations higher than those of pseudo-thermal light [17–21]. We call these sources "super-thermal" since their intensity fluctuates more than that of thermal ones. There are different ways to produce super-thermal sources. Some years ago, we demonstrated that the second-harmonics of a pseudo-thermal light displays super-thermal statistics [22,23]. However, the generation of this kind of light is not always very efficient since it is based on a nonlinear process in which energy- and phase-matching conditions must be fulfilled [24]. In this work, we address a different strategy to generate super-thermal light field based on linear processes in two diffusers instead of just one [25–28]: the pseudo-thermal light produced by the first diffuser is properly selected by a pin-hole and sent to the second diffuser. Such a scheme has already been investigated in the past, even if a general characterization of the obtained field is still missing [29]. In our work, we derive the statistical properties for the general case in which μ_f spatial modes are

selected at the output of the first disk and μ_s modes at the exit of the second one. This choice allows a better comparison of the super-thermal statistics with the pseudo-thermal one.

At variance with the large part of the experimental works on doubly-scattered light present in the literature that has been realized at the single-photon level [26,30,31] with single-photon detectors, in our investigation, we operate in the mesoscopic intensity regime by employing photon-number-resolving (PNR) detectors. The choice of this regime allows us to thoroughly study the statistical properties of light in terms of measurable quantities. We can calculate the photon-number distribution for detected photons, which, in many applications, is the most qualifying feature of the employed optical states [32–38]. As an example, we can consider employing this kind of light in the field of quantum information science: thermal or super-thermal states, superimposed to quantum states of light [39], can be used to encode information, such as in the protocol we presented in Refs. [40,41]. The mesoscopic intensity regime is also potentially interesting for applications to imaging thanks to the use of arrays of PNR detectors [42].

In the following, we derive the general expression of the photon-number statistics corresponding to the generated super-thermal light that we will call the "speckled-speckle" field hereafter. Then, we investigate some quantities based on the first two moments of the distributions to put in evidence the potentialities of this light source, especially in view of possible applications in the imaging context. In particular, we consider the second-order Glauber autocorrelation function and the cross-correlation coefficient. We show that the calculation of these two quantities is useful for the characterization of the speckled-speckle field since it allows the determination of the involved spatial modes.

2. Materials and Methods

When a coherent light beam, such as a laser beam, impinges on a diffuser, it produces a speckle field composed of many spatial modes, the speckles, that are the result of the constructive interference of the radiation coming from the small scattering centers within the area of the diffuser illuminated by the laser beam [29]. The statistical distribution of the speckle field is given by a thermal distribution $p_{\text{th}}(I) = (1/\langle I \rangle) \exp(-I/\langle I \rangle)$, where $\langle I \rangle$ is the mean intensity of the speckle field.

If we now select a portion of the speckle field with a pin-hole, so that only a single speckle passes through, and rotate the diffuser, the statistical distribution of the light at the exit of the pin-hole results thermal. Conversely, by selecting more than one speckle with the pin-hole, the statistical distribution becomes multi-mode thermal. By assuming that all the selected μ modes, i.e., the speckles, in the light are equally populated, the probability density function corresponding to the collected light can be expressed as [43]

$$p_\mu(I) = \frac{\mu^\mu I^{\mu-1}}{\Gamma(\mu)\langle I \rangle^\mu} \exp\left[-\mu \frac{I}{\langle I \rangle}\right], \tag{1}$$

where μ is the effective number of speckles, $\langle I \rangle = \mu I_0$ is the mean intensity of the speckle field, I_0 being the mean intensity of each speckle, and Γ is the Γ-function. By applying to Equation (1) the semiclassical theory of photodetection [43], the probability distribution of detected photons, m, for a PNR detector

$$P_\mu(m) = \binom{m+\mu-1}{\mu-1} \left(1 + \frac{\langle m \rangle}{\mu}\right)^{-\mu} \left(1 + \frac{\mu}{\langle m \rangle}\right)^{-m} \tag{2}$$

can be obtained, in which $\langle m \rangle$ is the total mean number of detected photons. If μ_f speckles of this first speckle field are now selected through a pin-hole and sent to a second diffuser,

at whose output a second pin-hole selects μ_s speckles, the general expression of the density function corresponding to the obtained speckled-speckle field is [29]

$$p_{sth}(I) = \frac{2(\mu_f\mu_s)^{\frac{(\mu_f+\mu_s)}{2}}}{\langle I\rangle\Gamma(\mu_s)\Gamma(\mu_f)}\left(\frac{I}{\langle I\rangle}\right)^{\frac{(\mu_f+\mu_2-2)}{2}} K_{|\mu_f-\mu_s|}\left(2\sqrt{\mu_s\mu_f\frac{I}{\langle I\rangle}}\right), \tag{3}$$

where $K_{|\mu_f-\mu_s|}$ is the $|\mu_f-\mu_s|$-order modified Bessel function of the second kind.

By again applying the semiclassical theory of photodetection to Equation (3), we obtain the probability distribution of detected photons

$$\begin{aligned} P_{\mu_f,\mu_s}(m) &= \frac{1}{\Gamma(\mu_f)\Gamma(\mu_s)m!}\left(\frac{\mu_f\mu_s}{\langle m\rangle}\right)^{\frac{(\mu_f+\mu_s-|\mu_f-\mu_s|)}{2}} \\ &\times \Gamma\left(\frac{(2m+\mu_f+\mu_s-|\mu_f-\mu_s|)}{2}\right)\Gamma\left(\frac{(2m+\mu_f+\mu_s+|\mu_f-\mu_s|)}{2}\right) \\ &\times U\left(\frac{(2m+\mu_f+\mu_s+|\mu_f-\mu_s|)}{2}, 1-|\mu_f-\mu_s|, \frac{\mu_f\mu_s}{\langle m\rangle}\right), \end{aligned} \tag{4}$$

where $U(a,b,c)$ is the confluent hypergeometric function of the second kind.

We notice that the expression in Equation (4) is more general than that reported on Ref. [26], where μ_s is considered equal to 1.

From Equation (4) we can obtain the first two moments of the distribution, from which we can calculate relevant statistical quantities, such as the second-order autocorrelation function. We obtain

$$\langle m\rangle = \mu_s\langle m_s\rangle \tag{5}$$

$$\sigma^2(m) = \left(\frac{1}{\mu_f}+\frac{1}{\mu_s}+\frac{1}{\mu_f\mu_s}\right)\langle m\rangle^2+\langle m\rangle, \tag{6}$$

$\langle m_s\rangle$ being the mean value associated with each speckle coming from the second diffuser. It is worth noting that both in Equations (4) and (6), the expressions are symmetric with respect to the number of modes, regardless of whether they come from either the first diffuser or the second one. From Equations (5) and (6), it is possible to calculate the second-order autocorrelation function for detected photons [44]

$$g^2(m) = \frac{\langle m^2\rangle}{\langle m\rangle^2} = \frac{\sigma^2(m)}{\langle m\rangle^2}+\frac{\langle m\rangle^2}{\langle m\rangle^2} = \left(1+\frac{1}{\mu_f}\right)\left(1+\frac{1}{\mu_s}\right)+\frac{1}{\langle m\rangle}, \tag{7}$$

where we note that the last term on the right side comes from taking detection into account. In fact, the second-order autocorrelation function of the incident photons, $g^2(n)$, would only depend on the numbers of speckles μ_f and μ_s and not on the mean value

$$g^2(n) = \left(1+\frac{1}{\mu_f}\right)\left(1+\frac{1}{\mu_s}\right). \tag{8}$$

Since the second-order autocorrelation function is the quantity that is evaluated in correlation-based imaging schemes, we investigate its dependence on the number of modes. In Figure 1, we plot $g^2(m)$ as a function of the mean value for $\mu_f = 1$ and different choices of μ_s (colored dots). In the same figure, we plot $g^2(m)$ in the case of single-mode thermal light (dashed gray curve). We note that there are choices of μ_s larger than 1 for which superthermal light is definitely more correlated than thermal light, thus proving that the speckled-speckle field can be a useful resource in all the situations in which having high fluctuations is important.

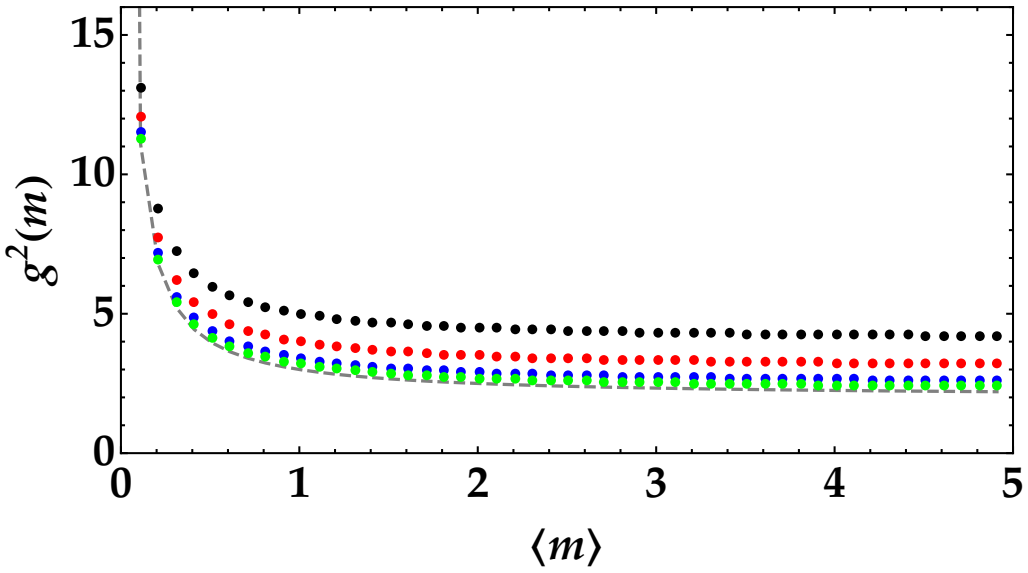

Figure 1. Second-order autocorrelation function $g^2(m)$ as a function of the mean number of photons for $\mu_f = 1$ and different values of μ_s. Different colors refer to different choices of μ_s. From top to bottom: black to $\mu_s = 1$, red to $\mu_s = 2$, blue to $\mu_s = 5$, and green to $\mu_s = 10$. The dashed gray curve corresponds to a single-mode thermal state of light.

We also note that even in the case $\mu_f = \mu_s = 2$, super-thermal light is still more correlated than a thermal light with $\mu = 1$.

This fact can be emphasized by dividing the light beam at a balanced beam splitter (BS) and then calculating the correlation between the two BS outputs. We define the cross-correlation coefficient [45]

$$\Gamma = \frac{\langle (m_1 - \langle m_1 \rangle)(m_2 - \langle m_2 \rangle) \rangle}{\sqrt{\sigma^2(m_1)\sigma^2(m_2)}}, \tag{9}$$

where $\langle m_{1,2} \rangle$ and $\sigma^2(m_{1,2})$ are the mean value and the variance in the $j = 1,2$ BS arm, respectively.

Assuming a balanced BS, for the super-thermal light described by the distribution of detected photons in Equation (4), the correlation coefficient Γ reads

$$\Gamma = \frac{\left(\frac{1}{\mu_f} + \frac{1}{\mu_s} + \frac{1}{\mu_f \mu_s} \right) \langle m \rangle}{1 + \left(\frac{1}{\mu_f} + \frac{1}{\mu_s} + \frac{1}{\mu_f \mu_s} \right) \langle m \rangle}. \tag{10}$$

In Figure 2, we show Γ as a function of the mean value of detected photons for different choices of μ_f and μ_s. For a direct comparison, in the same figure, we plot the behavior of Γ in the case of a single-mode thermal state. As already noticed for g^2, superthermal light is more correlated than thermal light if the numbers of modes are small. Indeed, both μ_f and μ_s should be larger than 1 (i.e., $\mu_f = \mu_s = 5$) to give values of Γ lower than those corresponding to a thermal field. Actually, in the case of $\mu_f = \mu_s$, the boundary to a single-mode thermal field is reached for $\mu_f = \mu_s = 1 + \sqrt{2}$.

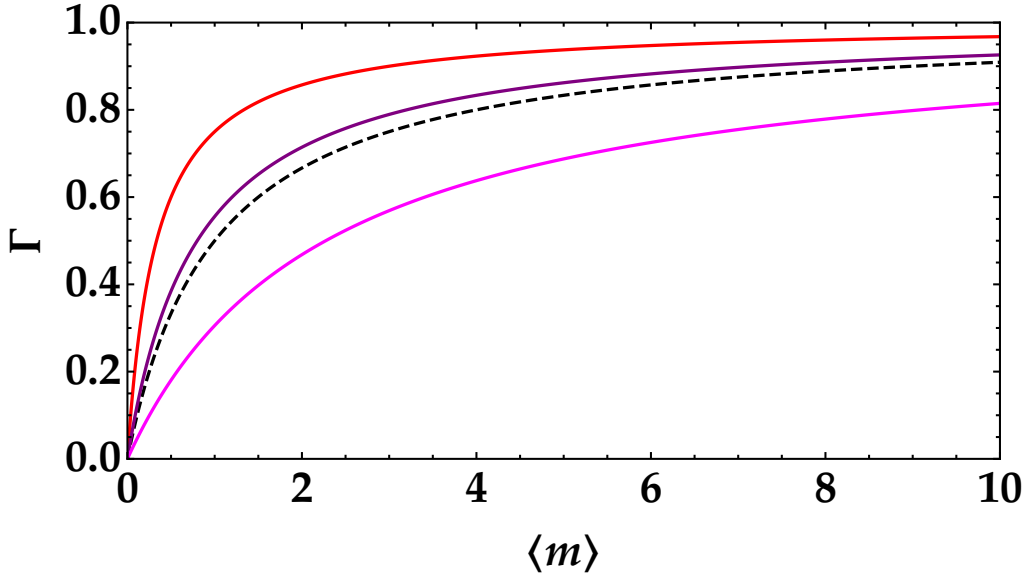

Figure 2. Cross-correlation coefficient Γ as a function of the mean number of detected photons at each of the outputs of the BS for different values of μ_f and μ_s. From top to bottom, red curve: $\mu_f = 1$ and $\mu_s = 1$; purple curve: $\mu_f = 2$ and $\mu_s = 2$; magenta curve: $\mu_f = 5$ and $\mu_s = 5$; dashed black curve: $\mu = 1$ for single-mode thermal state of light.

To summarize, both Equations (7) and (10) depend on the number of modes coming from both disks. This means that the calculation of both g^2 and Γ as a function of the mean value of the light is useful to extract information about the values of μ_f and μ_s by fitting the relations $g^2(m)$ and $\Gamma(m)$ with Equations (7) and (10), respectively.

In order to practically investigate such properties, we realized the experimental setup shown in Figure 3.

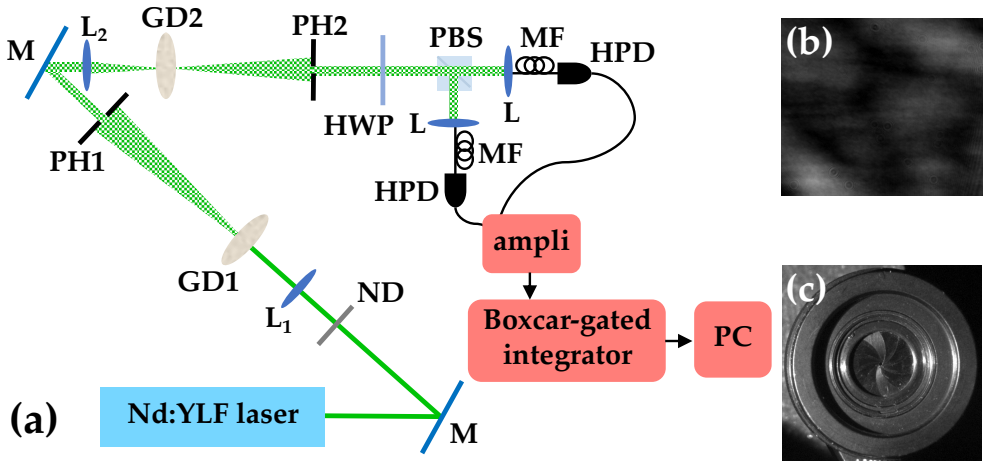

Figure 3. (**a**) Sketch of the experimental setup. M: mirror; ND: neutral density filter; L_1: 200-mm-focal length lens; L_2: 100-mm-focal length lens; GD1 and GD2: rotating ground-glass disks; PH1: first pin-hole; PH2: 150-µm-diameter pin-hole; HWP: half-wave plate; PBS: polarizing cube beam splitter; L: achromatic doublet; MF: multi-mode optical fiber; HPD: hybrid photodetector. (**b**) Typical single-shot image of the speckle field in correspondence of the position of PH1. (**c**) Picture of the first pin-hole PH1.

The ps-pulses (at 1047 nm) of a Nd:YLF laser regeneratively amplified at 500 Hz and frequency doubled at 523 nm were focused on a rotating ground-glass disk (GD1), having scattering centers of the order of 4 µm. A portion, roughly corresponding to a single speckle, of the generated speckle field was then selected by a pin-hole (PH1) placed in

far field and focused on a second ground-glass disk (GD2), characterized by scattering centers with the same size as those of GD1. Both disks were rotated in such a way that for the duration (∼5 ps) of a single pulse, they could be considered still, while they occupied different positions when different pulses were emitted. A portion of the generated speckled-speckle field (roughly corresponding to a single speckle) was then selected by a second pin-hole (PH2), whose diameter was equal to 150 µm. The light exiting the pin-hole was then divided at a polarizing cube BS placed behind a half-wave plate in order to finely control the balancing between the two arms. The two outputs were then focused by two achromatic doublets (L) into multi-mode fibers (MF) with a core diameter of 600 µm that delivered the light to two commercial PNR detectors operated at room temperature. More specifically, we used a pair of hybrid photodetectors (HPDs, mod. R10467U-40, Hamamatsu Photonics), whose output was amplified, synchronously integrated, and digitized. We performed measurements at different mean numbers of photons, attenuating the light by means of a variable neutral density filter (ND) placed in front of the first disk. We saved 100,000 acquisitions for each attenuation choice.

3. Results

By applying the self-consistent method already presented elsewhere [46–48], it is possible to extract the shot-by-shot number of detected photons from the output voltages of the detection chain. For the employed HPDs, the method consists of modeling the detection process in two steps: photodetection by the photocathode and amplification. The first process is given by a Bernoullian convolution, whereas the second one can be well approximated by the multiplication by a constant gain factor, whose value can be obtained by measuring the light at different values of the overall detection efficiency of the apparatus. This allows us to calculate all the relevant statistical quantities that characterize an optical state of light, such as those mentioned in the previous section. In particular, we have already noticed that the statistical distribution depends on the number of modes coming from the two diffusers and is symmetric with respect to μ_f and μ_s. We decided to extract the number of modes coming from the second disk by the calculation of the statistical quantities mentioned in the previous section and to determine the number of modes coming from the first disk by the direct measurement of the size of the speckles and of the size of the first pin-hole. To this aim, we first placed a coupled-charged device (CCD) camera (mod. DCU223M, Thorlabs, 1024 × 768 pixels, 4.65-µm pixel size) exactly in the position of the first pin-hole (PH1) and recorded some single-shot images (see Figure 3b for a typical single-shot image). From the analysis of the autocorrelation function of the images, we extracted the typical speckle size. Indeed, we estimated an area within 2σ equal to $A_{\mathrm{sp}} = 0.84 \pm 0.07$ mm^2. Second, we removed the CCD, placed the first pin-hole, and realized an imaging system to determine its aperture (see Figure 3c) by means of the same CCD camera. In this case, we obtained that the diameter of the first pin-hole was equal to $d_{\mathrm{PH1}} = 0.47 \pm 0.04$ mm and the corresponding area to $A_{\mathrm{PH1}} = 0.18 \pm 0.05$ mm^2. At first glance, the number of modes passing through this first pin-hole could be evaluated as the ratio of the area of the pin-hole to the area of the speckles. However, this definition of modes is only valid when a large number of speckles passes through the pin-hole. The opposite limit is the case, in which the pin-hole is much smaller than the typical speckle size. In this case, the value of μ_f can be considered equal to 1 [29]. The intermediate situation is very complex to deal with since the speckles are not rigid spheres but coherence areas propagating through a hole. Thus, assuming that the pin-hole is uniform and circular, and that the optical intensity pattern on the scattering spot is Gaussian-shaped, the following closed formula can be used to extract the effective number of modes passing through the pin-hole [29]

$$\mu_f = \left(\frac{A_{\mathrm{PH1}}}{A_{\mathrm{sp}}}\right)\left\{1 - \exp\left[-2\frac{A_{\mathrm{PH1}}}{A_{\mathrm{sp}}}\right]\left[I_0\left(\frac{2A_{\mathrm{PH1}}}{A_{\mathrm{sp}}}\right) + I_1\left(\frac{2A_{\mathrm{PH1}}}{A_{\mathrm{sp}}}\right)\right]\right\}^{-1}, \qquad (11)$$

where A_{sp} and A_{PH1} are the areas of speckles and pin-hole, respectively, while I_0 and I_1 are the zero- and first-order modified Bessel functions of the first kind. Applied to the measured values of speckles and pin-hole, Equation (11) returns a value $\mu_f = 1.22 \pm 0.07$.

Thanks to the independent determination of μ_f, by the calculation of the quantities in Equations (4), (7), and (10), it is possible to extract and compare the values of μ_s. First of all, we consider the reconstruction of the detected-photon distribution for two different mean values.

In Figure 4, we show the experimental data in semilogarithmic scale together with the theoretical fitting functions according to Equation (4), in which the value of μ_f is fixed, while that of μ_s is left as a fitting parameter. The values of μ_s obtained at the two different mean numbers of photons (see panels (a,b)) are very similar to each other, thus proving that the number of modes is independent of the mean value of light. The good quality of the fitting procedure is proved by the high values of the fidelity, which is defined as $f = \sum_{m=0}^{\overline{m}} \sqrt{P(m)P_{\text{theo}}(m)}$, where $P(m)$ and $P_{\text{theo}}(m)$ are the experimental and theoretical distributions, respectively, and the sum is extended up to the maximum detected-photon number, $\overline{m}$, above which the two distributions become negligible.

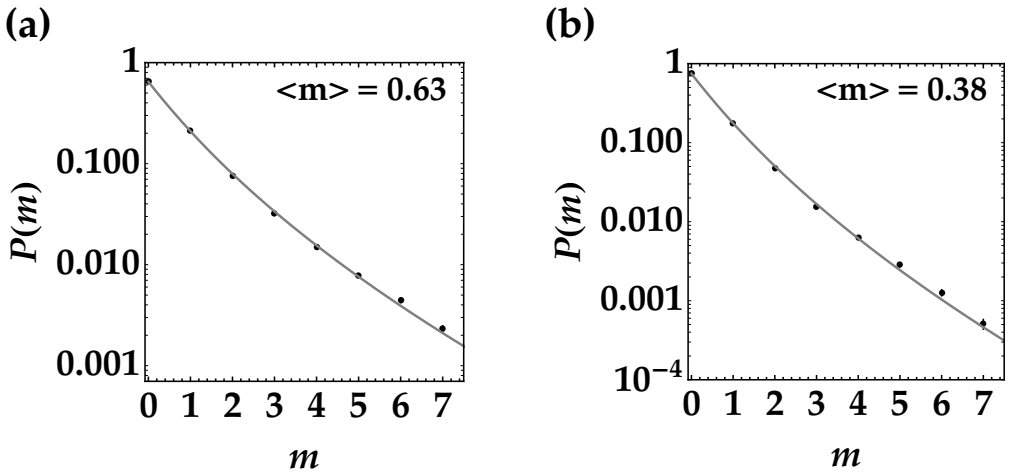

Figure 4. Detected-photon number distributions reconstructed at one BS output for two mean values of the speckled-speckle field. Black dots and error bars: experimental data; gray curves: theoretical fitting functions according to Equation (4), in which $\mu_f = 1.22$, while μ_s is the only fitting parameter. The obtained values are: $\mu_s = 1.74 \pm 0.02$ in panel (**a**) and $\mu_s = 1.76 \pm 0.02$ in panel (**b**). The corresponding values of fidelity are: $f = 0.9999$ and $f = 0.9999$, respectively.

To further investigate the independence of the number of modes from the mean value, we can also calculate the second-order autocorrelation function for detected photons.

In Figure 5, we show the behavior of g^2 as a function of the mean value for the two BS outputs. By fitting the data measured in the two BS arms according to the theoretical model in Equation (7), it is possible to extract the values of μ_s. Note that such values are constant in the investigated intensity range, as it is well evident from Figure 6, where the calculated values of μ_s as obtained by inverting Equation (7) applied to experimental data, are compared to the fitting values of Figure 5.

The small difference between the values of μ_s extracted from the two fits (see caption of Figure 5) may be ascribed to a non-perfect balancing of the two BS arms, which slightly differ from each other at low mean values. In particular, we note that the value extracted from panel (a) is similar (within 1σ) to the values extracted from the photon-number distributions. The slight discrepancy is due to the fact that μ_s, as calculated from g^2, is obtained by together considering the measurements performed at different mean values, while that obtained from each photon-number distribution is referred to a specific mean value.

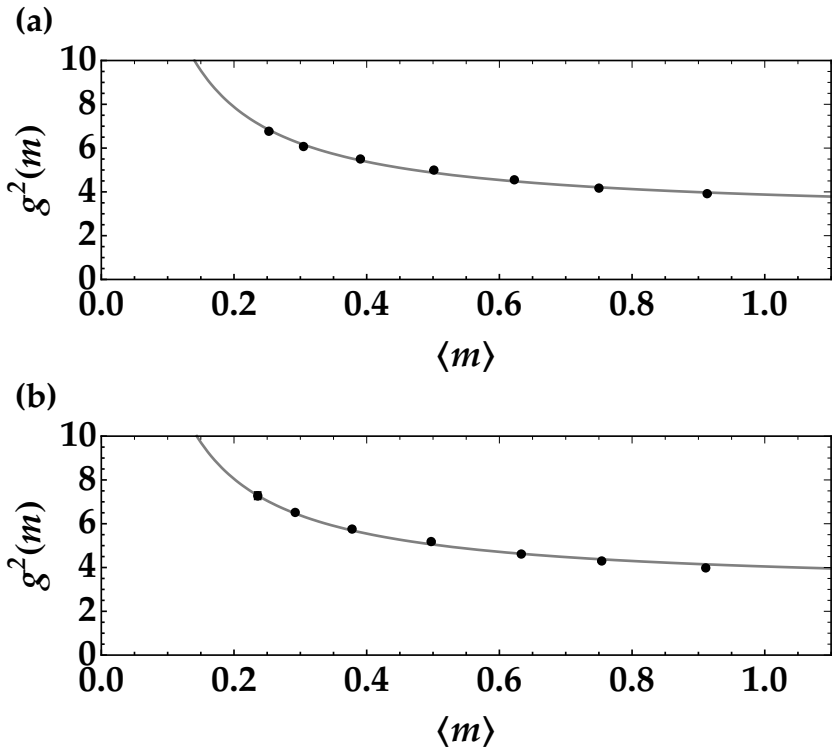

Figure 5. Second-order autocorrelation function $g^2(m)$ as a function of the mean number of detected photons reconstructed at the two BS outputs. Black dots and error bars: experimental data; gray curves: theoretical fitting functions according to Equation (7), in which $\mu_f = 1.22$, while μ_s is the only fitting parameter. The obtained values are: $\mu_s = 1.72 \pm 0.05$ in panel (**a**) and $\mu_s = 1.48 \pm 0.05$ in panel (**b**).

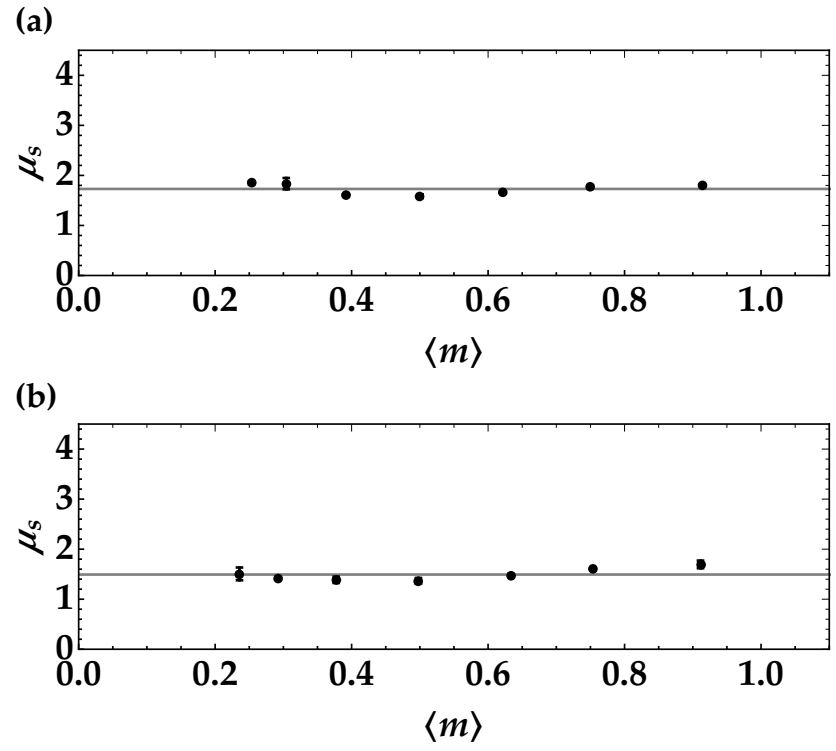

Figure 6. Values of μ_s obtained by inverting Equation (7) applied to the experimental data as a function of the mean number of detected photons reconstructed at the two BS outputs. Black dots and error bars: experimental data; gray lines: values of μ_s obtained from the fitting procedure applied to the data in Figure 5, namely, $\mu_s = 1.72$ in panel (**a**) and $\mu_s = 1.48$ in panel (**b**).

As a final comparison, we consider the case of the cross-correlation coefficient calculated between the two BS outputs. The experimental data are shown in Figure 7a together with the theoretical expectation according to Equation (10). Additionally, in this case, we kept the value of μ_f fixed and extracted that of μ_s from the fitting procedure. The good superposition of data on the theoretical curve proves again the correctness of the theoretical model. As expected, in this case, the value of the fitting parameter is $\mu_s = 1.69 \pm 0.06$, which represents an average between the values of μ_s obtained from g^2 for the two BS outputs. For a direct comparison, in the same plot, we also show the expected behavior in the case of a single-mode thermal state divided at a balanced BS. It is well evident that the use of super-thermal statistics instead of thermal guarantees larger photon-number correlations.

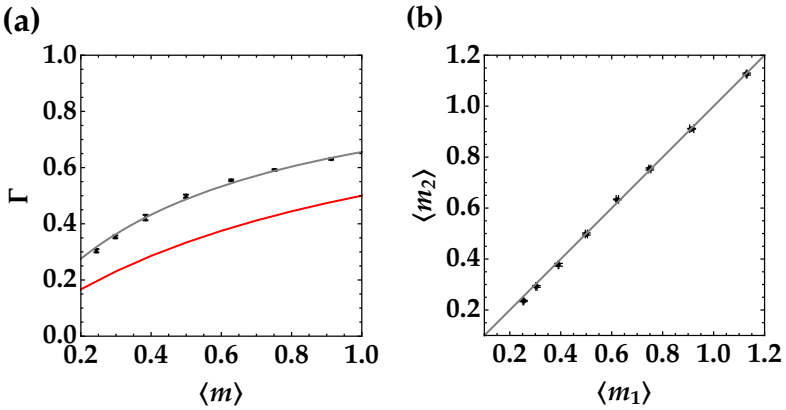

Figure 7. (**a**) Cross-correlation coefficient Γ as a function of the mean number of detected photons obtained as the average betwen the two BS outputs. Black dots and error bars: experimental data; red curve: theoretical model in the case of a single-mode thermal state; gray curve: theoretical fitting function according to Equation (10), in which $\mu_f = 1.22$, while μ_s is the only fitting parameter. The obtained value is: $\mu_s = 1.69 \pm 0.06$. (**b**) Black dots and error bars: mean number of photons detected at one BS output as a function of the mean number of photons detected at the other output. Gray line: diagonal $y = x$.

As already remarked, the small discrepancy between the two values of μ_s extracted from the autocorrelation function may be ascribed to the small imbalance between the two BS arms, which is more pronounced at small mean values, as it can be noticed in Figure 7b, where the mean numbers of photons detected at one BS output are shown as a function of those at the other output together with the diagonal $y = x$.

4. Discussion

The results presented in the previous section confirm that the developed model is in excellent agreement with the data. In particular, we can see that the different quantities used to estimate the number of modes collected at the output of the second disk are essentially equivalent. This is quite expected since all of them are based on the moments of the distribution in Equation (4), even if the distribution of the number of photons contains all the moments of the statistics, whereas the autocorrelation function g^2 and the cross-correlation Γ depend only on the first two moments. This difference may explain the small discrepancies between the obtained results. We verified that the number of modes is independent of the mean value of light, both considering the photon number distribution and the autocorrelation function. In fact, the experimental values of μ_s extracted from the fitting procedures in both cases coincide within 1σ. As to the difference between the values obtained at the two BS outputs, we argue that it is due to a slight imbalance between the light in the two arms. This is also demonstrated by the calculation of Γ, from which a value of μ_s was obtained that is an average between the values extracted from the calculation of g^2. As already specified in the Introduction, the preliminary characterization we carried on is important in itself for all those applications in the field of quantum information, in which

investigating the statistics of light is sufficient. For instance, this kind of light can find applications in novel communication protocols, such as those presented in Refs. [40,41]. The original scheme is based on the experimental quantification of nonclassicality of mesoscopic twin-beam states to transmit binary signals encoded in two single-mode pseudo-thermal states with different mean values. Interesting variations of this protocol could involve either the use of super-thermal states with different mean values or the alternate use of pseudo-thermal and super-thermal states with the same mean value. Moreover, this specific type of light can also be used in the context of imaging, where some other works exploiting super-thermal light have been recently published [31,49]. At variance with these investigations, we note that we performed our experiment in the pulsed regime with PNR detectors able to operate in the mesoscopic intensity domain. Finally, we observe that for imaging applications, it might be important to treat even more populated states of light and use macroscopic detectors, such as CCD cameras. To this end, more intense light states and less opaque diffusers may be desirable. Work is in progress in this direction. As an alternative to the macroscopic regime, imaging protocols involving super-thermal states can be implemented in the mesoscopic one thanks to the use of arrays of PNR detectors, such as complementary metal-oxide-semiconductor (CMOS) cameras having each pixel endowed with PNR capability [42].

5. Conclusions

In this paper, we have investigated, both theoretically and experimentally, the statistical properties of a classical light state that exhibits more fluctuations than a thermal state. We generated this light in the mesoscopic intensity regime by sending the laser pulses at 523 nm to a sequence of two rotating ground-glass disks and detecting the light exiting the second disk by means of PNR detectors. We characterized such optical states by reconstructing their photon-number statistics and calculating both the second-order autocorrelation function and the cross-correlation coefficient between the outputs of a BS in terms of measurable quantities, i.e., detected photons. All the statistical quantities depend on the numbers of modes μ_f and μ_s selected at the exit of the first and the second disk, respectively, and result as symmetric in the exchange of the modes. The possibility to express the statistics in an analytic form allowed us to easily compare super-thermal and pseudo-thermal lights and to better investigate the conditions under which the fluctuations exhibited by the former are higher than those shown by the latter. The good quality of the results and their agreement with the theoretical model suggest the potential usefulness of this kind of light for applications, such as imaging, in which the existence of correlations represents the main requirement.

Author Contributions: Conceptualization, A.A. and M.B.; methodology, A.A. and M.B.; validation, A.A. and C.B.; investigation, A.A. and C.B.; writing—original draft preparation, A.A., C.B. and M.B.; writing—review and editing, A.A., C.B. and M.B. All authors have read and agreed to the published version of the manuscript.

Funding: This research received no external funding.

Institutional Review Board Statement: Not applicable.

Informed Consent Statement: Not applicable.

Data Availability Statement: Data underlying the results presented in this paper are not publicly available at this time but may be obtained from the author upon reasonable request.

Acknowledgments: The authors thank Alberto Parola, Silvia Cassina, and Gabriele Cenedese (University of Insubria) for fruitful discussions.

Conflicts of Interest: The authors declare no conflict of interest.

Abbreviations

The following abbreviations are used in this manuscript:

PNR	photon-number-resolving
HPD	hybrid photodetector
BS	beam splitter
CCD	coupled-charged device
CMOS	complementary metal-oxide-semiconductor

References

1. Valencia, A.; Scarcelli, G.; D'Angelo, M.; Shih, Y.H. Two-photon imaging with thermal light. *Phys. Rev. Lett.* **2005**, *94*, 063601. [CrossRef] [PubMed]
2. Ferri, F.; Magatti, D.; Gatti, A.; Bache, M.; Brambilla, E.; Lugiato, L.A. High-Resolution Ghost Image and Ghost Diffraction Experiments with Thermal Light. *Phys. Rev. Lett.* **2005**, *94*, 183602. [CrossRef] [PubMed]
3. Martienssen, W.; Spiller, E. Coherence and fluctuations in light beams. *Am. J. Phys.* **1964**, *32*, 919–926. [CrossRef]
4. Arecchi, F.T. Measurement of the Statistical Distribution of Gaussian and Laser Sources. *Phys. Rev. Lett.* **1995**, *15*, 912. [CrossRef]
5. Gatti, A.; Brambilla, E.; Bache, M.; Lugiato, L.A. Correlated imaging, quantum and classical. *Phys. Rev. A* **2004**, *70*, 013802. [CrossRef]
6. Gatti, A.; Brambilla, E.; Bache, M.; Lugiato, L.A. Ghost imaging with thermal light: Comparing entanglement and classical correlation. *Phys. Rev. Lett.* **2004**, *93*, 093602. [CrossRef]
7. Bache, M.; Brambilla, E.; Gatti, A.; Lugiato, L.A. Ghost imaging using homodyne detection. *Phys. Rev. A* **2004**, *70*, 023823. [CrossRef]
8. Bache, M.; Brambilla, E.; Gatti, A.; Lugiato, L.A. Ghost imaging schemes: Fast and broadband. *Opt. Express* **2004**, *12*, 6067. [CrossRef]
9. Crosby, S.; Castelletto, S.; Aruldoss, C.; Scholten, R.E.; Roberts, A. Modelling of classical ghost images obtained using scattered light. *New J. Phys.* **2007**, *9*, 285. [CrossRef]
10. Ferri, F.; Magatti, D.; Lugiato, L.A.; Gatti, A. Differential Ghost Imaging. *Phys. Rev. Lett.* **2010**, *104*, 253603. [CrossRef]
11. Allevi, A. Mesoscopic States of Light for the Detection of Weakly Absorbing Objects. *Photonics* **2022**, *9*, 819. [CrossRef]
12. Mudry, E.; Belkebir, K.; Girard, J.; Savatier, J.; Le Moal, E.; Nicoletti, C.; Allain, M.; Sentenac, A. Structured illumination microscopy using unknown speckle patterns. *Nat. Photon.* **2012**, *6*, 312–315. [CrossRef]
13. Kulkarni, R.; Pal, P.; Banoth, E. Spatio-temporal analysis of dynamic speckle patterns using singular value decomposition. *Opt. Lasers Eng.* **2021**, *142*, 106588. [CrossRef]
14. Erkmen, B.I.; Shapiro, J.H. Signal-to-noise ratio of Gaussian-state ghost imaging. *Phys. Rev. A* **2009**, *79*, 023833. [CrossRef]
15. Iskhakov, T.; Allevi, A.; Kalashnikov, D.A.; Sala, V.G.; Takeuchi, M.; Bondani, M.; Chekhova, M. Noise reduction measurements and new ghost imaging protocols. *Eur. Phys. J. Spec. Top.* **2011**, *199*, 127–138. [CrossRef]
16. Ragy, S.; Adesso, G. Nature of light correlations in ghost imaging. *Sci. Rep.* **2012**, *2*, 651. [CrossRef]
17. Dove, J.; Shapiro, J.H. Speckled speckled speckle. *Opt. Express* **2020**, *28*, 22105. [CrossRef]
18. Bromberg, Y.; Cao, H. Generating non-Rayleigh speckles with tailored intensity statistics. *Phys. Rev. Lett.* **2014**, *112*, 213904. [CrossRef]
19. Bender, N.; Yilmaz, H.; Bromberg, Y.; Cao, H. Customizing speckle intensity statistics. *Optica* **2018**, *5*, 595–600. [CrossRef]
20. Alves, S.B.; Cavalcante, H.L.D.S.; de Oliveira, G.F., Jr.; Passerat de Silans, T.; Vidal, I.; Chevrollier, M.; Oriá, M. Controlling the intensity statistics of speckle patterns: From normal to subthermal or superthermal distributions. *Phys. Rev. A* **2019**, *99*, 033838. [CrossRef]
21. Li, Z.; Nie, X.; Yang, F.; Liu, X.; Liu, D.; Dong, X.; Zhao, X.; Peng, T.; Zubairy, M.S.; Scully, M.O. Sub-Rayleigh second-order correlation imaging using spatially distributive colored noise speckle patterns. *Opt. Express* **2021**, *29*, 19621–19630. [CrossRef]
22. Allevi, A.; Bondani, M. Direct detection of super-thermal photon-number statistics in second-harmonic generation. *Opt. Lett.* **2015**, *40*, 3089–3092. [CrossRef]
23. Allevi, A.; Cassina, S.; Bondani, M. Super-thermal light for imaging applications. *Quantum Meas. Quantum Metrol.* **2017**, *4*, 26–34. [CrossRef] [PubMed]
24. Boyd, R.W. *Nonlinear Optics*, 3rd ed.; Academic Press: Burlington, MA, USA; San Diego, CA, USA; London, UK, 2008; pp. 84–91. [CrossRef] [PubMed]
25. O' Donnell, K.A. Speckle statistics of doubly scattered light. *J. Opt. Soc. Am.* **1982**, *72*, 1459–1463. [CrossRef]
26. Newman, D. K distributions from doubly scattered light. *J. Opt. Soc. Am. A* **1985**, *2*, 22–26.
27. Barakat, R.; Salawitch, R.J. Second and fourth-order statistics of doubly scattered speckle. *Opt. Acta Int. J. Opt.* **1986**, *33*, 79–89. [CrossRef]
28. Gori, F.; Santarsiero, M. Spatial superbunching of light. Model sources. *Opt. Lett.* **2019**, *44*, 4012–4015. [CrossRef]
29. Goodman, J.W. *Speckle Phenomena in Optics: Theory and Applications*; Roberts & Company: Greenwood Village, CO, USA, 2007. [CrossRef]
30. Yoshimura, T.; Fujiwara, K. Statistical properties of doubly scattered image speckle. *J. Opt. Soc. Am. A* **1992**, *9*, 91–95. [CrossRef]

31. Zhou, Y.; Zhang, X.; Wang, Z.; Zhang, F.; Chen, H.; Zheng, H.; Liu, J.; Li, F.L.; Xu, Z. Superbunching pseudothermal light with intensity modulated laser light and rotating groundglass. *Opt. Commun.* **2019**, *437*, 330–336.
32. Avenhaus, M.; Coldenstrodt-Ronge, H.B.; Laiho, K.; Mauerer, W.; Walmsley, I.A.; Silberhorn, C. Photon Number Statistics of Multimode Parametric Down-Conversion. *Phys. Rev. Lett.* **2008**, *101*, 053601. [CrossRef]
33. Peřina, J., Jr.; Hamar, M.; Michálek, V.; Haderka, O. Photon-number distributions of twin beams generated in spontaneous parametric down-conversion and measured by an intensified CCD camera. *Phys. Rev. A* **2012**, *85*, 023816. [CrossRef]
34. Hartmann, S.; Friedrich, F.; Molitor, A.; Reichert, M.; Elsäßer, W.; Walser, R. Tailored quantum statistics from broadband states of light. *New J. Phys.* **2015**, *17*, 043039. [CrossRef]
35. Bina, M.; Allevi, A.; Bondani, M.; Olivares, S. Phase-reference monitoring in coherent-state discrimination assisted by a photon-number resolving detector. *Sci. Rep.* **2016**, *6*, 26025. [CrossRef]
36. Bina, M.; Allevi, A.; Bondani, M.; Olivares, S. Homodyne-like detection for coherent state-discrimination in the presence of phase noise. *Opt. Express* **2017**, *25*, 10685–10692. [CrossRef]
37. Straka, I.; Mika, J.; Ježek, M. Generator of arbitrary classical photon statistics. *Opt. Express* **2018**, *26*, 8998–9010. [CrossRef]
38. Cheng, R.; Zhou, Y.; Wang, S.; Shen, M.; Taher, T.; Tang, H.X. A 100-pixel photon-number-resolving detector unveiling photon statistics. *Nat. Photon.* **2023**, *17*, 112–119. [CrossRef]
39. Allevi, A.; Bondani, M. Multi-mode twin-beam states in the mesoscopic intensity domain. *Phys. Lett. A* **2022**, *423*, 127828. [CrossRef]
40. Allevi, A.; Bondani, M. Novel scheme for secure data transmission based on mesoscopic twin beams and photon-number-resolving detectors. *Sci. Rep.* **2022**, *12*, 15621. [CrossRef]
41. Allevi, A.; Bondani, M. Feasibility of a Novel Quantum Communication Protocol in Jerlov Type I Water. *Entropy* **2023**, *25*, 16. [CrossRef]
42. Available online: https://www.hamamatsu.com/eu/en/product/cameras/qcmos-cameras/C15550-20UP.html (accessed on 31 March 2023). [CrossRef]
43. Mandel, L.; Wolf, E. *Optical Coherence and Quantum Optics*; Cambridge University Press: Cambridge, UK, 1995. [CrossRef]
44. Allevi, A.; Olivares, S.; Bondani, M. Measuring high-order photon-number correlations in experiments with multimode pulsed quantum states. *Phys. Rev. A* **2012**, *85*, 063835. [CrossRef]
45. Allevi, A.; Bondani, M.; Andreoni, A. Photon-number correlations by photon-number resolving detectors. *Opt. Lett.* **2010**, *35*, 1707–1709.
46. Bondani, M.; Allevi, A.; Agliati, A.; Andreoni, A. Self-consistent characterization of light statistics. *J. Mod. Opt.* **2009**, *56*, 226–231.
47. Allevi, A.; Bondani, M. Statistics of twin-beam states by photon-number resolving detectors up to pump depletion. *J. Opt. Soc. Am. B* **2014**, *31*, B14–B19. [CrossRef]
48. Allevi, A.; Bondani, M. Nonlinear and quantum optical properties and applications of intense twin-beams. *Adv. At. Mol. Opt. Phys.* **2017**, *66*, 49–110. [CrossRef] [PubMed]
49. Liu, J.; Zhuang, R.; Zhang, X.; Wei, C.; Zheng, H.; Zhou, Y.; Chen, H.; He, Y.; Xu, Z. Simple and efficient way to generate superbunching pseudothermal light. *Opt. Commun.* **2021**, *498*, 127264. [CrossRef] [PubMed]